

Zeroes and Extrema of Functions via Random Measures

Athanasios C. Micheas
 Department of Statistics
 University of Missouri
 email: micheasa@missouri.edu

November 14, 2025

Abstract

We present methods that provide all zeroes and extrema of a function that do not require differentiation. Using point process theory, we are able to describe the locations of zeroes or maxima, their number, as well as their distribution over a given window of observation. The algorithms in order to accomplish the theoretical development are also provided, and they are exemplified using many illustrative examples, for real and complex functions.

Keywords: Function extrema and zeroes; Optimization; Poisson point process; Random counting measures; Riemann's ζ function

MSC Classification: Primary: 60G55, Secondary: 90C23, 90C26

1 Introduction

Perhaps one of the most fundamental problems in mathematics is finding when the function assumes the value zero or where it achieves its extreme (maximum and minimum) values. It is astonishing to think how Sir Issac Newton's method withstood the test of time, and is still employed as we speak, in every mathematical discipline. Over the past four centuries, scientists have made many improvements to the original method, including introducing stochasticity. Although it has its difficulties and limitations, it has been the standard method to employ, since it involves one of the easiest and well understood concepts, that of the tangent via a Taylor expansion.

In this paper, we propose a novel method that provides all zeroes or the extrema of a function and their number, simultaneously, that does not suffer the usual problems of existing methods in the literature. There is a vast collection of papers and textbooks on general optimizations methods, with some recent published works including [37], [39], [6], [26], [18], [5], [40] and the references therein.

To formulate the ideas mathematically, let \mathbb{M} denote the real numbers \mathfrak{R} or the complex plane \mathbb{C} , and let $\mathcal{B}(\mathbb{X})$ denote the Borel sets of a space \mathbb{X} , using the topology induced by an

appropriate metric, depending on \mathbb{X} . In what follows, we consider a general function space

$$\mathcal{F}_{\mathbb{M}}^{\mathbb{M}^p} = \{f : \mathbb{M}^p \rightarrow \mathbb{M}, f \text{ continuous in } (\mathbb{M}, \mathcal{B}(\mathbb{M}))\}, \quad (1)$$

where we will assume that $\mathcal{F}_{\mathbb{M}}^{\mathbb{M}^p}$ is Hilbert, based on an inner product ρ . Then, we can immediately equip $\mathcal{F}_{\mathbb{M}}^{\mathbb{M}^p}$ with the induced norm

$$\|f\|_{\rho} = \sqrt{\rho(f, f)}, \quad (2)$$

and distance

$$d(f_1, f_2) = \|f_1 - f_2\|_{\rho} = \sqrt{\rho(f_1 - f_2, f_1 - f_2)}, \quad (3)$$

so that $\mathcal{F}_{\mathbb{M}}^{\mathbb{M}^p}$ becomes a normed vector (linear) space and $(\mathcal{F}_{\mathbb{M}}^{\mathbb{M}^p}, d)$ is a metric space.

Now since we do not know locations in the set of zero points of f , nor do we know how many of them there are, we can think of this set as the realization of random set that requires estimation or approximation. Specifically, the set of zeroes of f can be described by the deterministic set

$$\Xi_f = \{\xi \in \mathcal{X} \subset \mathbb{M}^p : f(\xi) = 0\}, \quad (4)$$

which has unknown elements and unknown cardinality $\#(\Xi_f)$. In order to describe the stochastic process that yields realizations of elements from Ξ_f , we naturally turn to point process (PP) theory. A point process is a random collection of points from a space \mathcal{X} , which is also random in number, and therefore, it offers an appealing framework to help us build the theory required to approximate the set Ξ_f .

We call the new method Point Process Zeroes (PPZ). The proposed approach utilizes point process theory and has the following characteristics:

- It is intuitively appealing, enjoys great interpretation and is easy to use.
- The PPZ provides all unknown zeroes of a given function and their number, at the same time, over a bounded window of observation, and in a single realization of the point process.
- The PPZ provides all unknown points of extrema (points where the derivative is zero) and the function maximum/minimum value, at the same time, based on a single realization of the point process over a bounded window of observation.
- Existing methods attempt to approach iteratively a single zero or point of extrema, and are often locked into local characteristics of the target function (e.g., simulated annealing) or do not converge. The PPZ does not suffer any of these difficulties.
- The PPZ does not require and it is not affected by starting values.
- The methods can be employed in any dimensional space, since they scale easily to higher dimensions by construction.
- The methods do not require differentiation of the given function to find its zeroes or extrema.

- The function under consideration must satisfy only mild conditions, such as continuity and being uniformly bounded over the window of observation.

For foundations, modeling, applications, computation methods and evaluation of point process models we refer to the texts by [24], [12], [4], [44], [28], [30], [35], [36], [15], [16], [23], [19], [11], [42], [17] and [2]. Some recent papers exploring general methodologies, applications and simulations of such processes include [21], [48], [38], [29], [13], [33], [49], [10], [43], [3], [8], [46], [1], [27], [47], [45], [14], [25], [20], [34], and the references therein.

The paper proceeds as follows; in Section 2 we introduce the new method for finding zeroes and study its theoretical properties with respect to the number of zeroes and their locations. Generalizations to multidimensional, and vector valued functions are also presented. Implementation and examples are presented in Section 3, including the main PPZ algorithm and its adaptive version that allows us to get as close to a zero or point of extrema as we wish. Many illustrative examples are also presented for real and complex functions. Concluding remarks are given in the last section.

2 Zeroes of Functions via Random Measures

Consider a probability space (Ω, \mathcal{A}, P) , and let \mathbb{N}^{lf} denote the collection of all locally finite counting measures on $\mathcal{X} \subset \mathbb{M}^p$, where if $\varphi \in \mathbb{N}^{lf}$ and $\mathcal{W} \in \mathcal{B}(\mathcal{X})$, then $\varphi(\mathcal{W})$ denotes the number of points in the set \mathcal{W} , also known as the window of observation. In order to define a random counting measure we create a measurable space based on a σ -field of subsets of \mathbb{N}^{lf} .

In particular, consider \mathcal{N} , the generated σ -field from the collection of sets of the form $\{\varphi \in \mathbb{N}^{lf} : \varphi(\mathcal{W}) = n\}$, for all $\mathcal{W} \in \mathcal{B}(\mathcal{X})$ and all $n \in \mathbb{N} = \{0, 1, 2, \dots\}$, so that $(\mathbb{N}^{lf}, \mathcal{N}^{lf})$ is a measurable space. Then a mapping N from (Ω, \mathcal{A}, P) into $(\mathbb{N}^{lf}, \mathcal{N}^{lf})$ can be thought of as a random object $N(\omega)(\cdot) = \varphi(\cdot)$, that yields counting measures φ for different $\omega \in \Omega$ and hence it is a random counting measure. The induced probability measure $\Pi_N(Y) = P(N \in Y) = P(N^{-1}(Y))$, describes the probability distribution of N and can be used to compute probabilities over sets $Y \in \mathcal{N}^{lf}$, where each element of Y is a counting measure.

In order to appreciate the usefulness of this construction, consider a countable set of events $S = \{\mathbf{x}_1, \mathbf{x}_2, \dots\}$, $\mathbf{x}_i \in \mathcal{X}$. Knowing $\varphi(\mathcal{W})$ for all $\mathcal{W} \in \mathcal{B}(\mathcal{X})$ is equivalent to knowing the locations of all points in S . Indeed, $\varphi(\mathcal{W}) = \sum_{i=1}^{+\infty} I(\mathbf{x}_i \in \mathcal{W})$, $\forall \mathcal{W} \in \mathcal{B}(\mathcal{X})$, so that knowing the locations implies that we know the counting measure φ . Conversely, \mathbf{x} is a point from S if $\varphi(\{\mathbf{x}\}) > 0$ and the point is distinct if $\varphi(\{\mathbf{x}\}) = 1$. Now if φ is a realization of a random counting measure, i.e., $\varphi = N(\omega)$, for some $\omega \in \Omega$, then this important relationship between φ and S defines a random collection of points (a countable random set) N , known as a point process.

We will exploit this representation of collections of points from the space \mathcal{X} in order to find zeroes or extrema of a function $f \in \mathcal{F}_{\mathbb{M}^p}$. Specifically, the set of zeroes of f can be described by the set Ξ_f which is possibly uncountable for $\mathcal{X} = \mathbb{M}^p$, but will be assumed to be countable over $\mathcal{X} \subset \mathbb{M}^p$. Therefore, the cardinality $\#(\Xi_f)$ of Ξ_f denotes the number of zeroes of f in \mathcal{X} , and could be any natural integer in \mathbb{N} .

Since we do not know neither the number of zeroes $\#(\Xi_f)$ nor their locations, the countable set Ξ_f will be treated as a realization of a random counting measure N , such that N has counting variables $N(\mathcal{W}) = \#(N \cap \mathcal{W})$, for any $\mathcal{W} \in \mathcal{B}(\mathcal{X})$, i.e., it satisfies

$$N(\mathcal{W}) = \sum_{\mathbf{x} \in N} I(\mathbf{x} \in \mathcal{W}). \quad (5)$$

Note that we do not concern ourselves with the multiplicity of a zero, but rather we want to find their number and their locations over a given bounded window $\mathcal{W} \in \mathcal{B}(\mathcal{X})$, and do this simultaneously. An important consideration here, is that the zero locations will be assumed to be independent of each other. We discuss relaxing this assumption, i.e., replace independence via conditional independence in our concluding remarks. We briefly discuss the classic choice of random measure for independent events next.

2.1 Poisson Point Processes

The most important point process model for independent events is the Poisson process (e.g., [15], [16], [23], [19], [11], [17] and [2]). It is often referred to as being “completely at random” or as a point process with “no interactions”, since the number of events (and the events themselves) over disjoint sets are independent of each other.

In what follows, let μ_p denote Lebesgue measure over \mathbb{M}^p . Consider a window of observation $\mathcal{W} \subset \mathbb{M}^p$, and suppose that we observe n points (events) $\varphi_n = \{\mathbf{x}_i\}_{i=1}^n$ from a point process N , with $\mathbf{x}_i \in \mathcal{W}$. In order to model this collection of points we consider the inhomogeneous Poisson point process (IPPP), which assumes that the random variables (counting variables) $N(B)$, $B \subseteq \mathcal{W}$, are distributed as Poisson and that the counts are independent over any finite collection of disjoint regions.

In particular, the expected number of events $\Lambda(B) = E[N(B)]$, known as the intensity measure, is the mean of a Poisson random variable, i.e., $N(B) \sim Pois(\Lambda(B))$. When Λ is absolutely continuous with respect to μ_p , an appeal to the Radon-Nikodym theorem yields

$$\Lambda(B) = E[N(B)] = \int_B \lambda(\mathbf{x}) \mu_p(d\mathbf{x}), \quad (6)$$

where $\lambda(\mathbf{x})$ is known as the intensity function and it uniquely determines the distribution of the IPPP N . The special case where $\lambda(\mathbf{x}) = \lambda$ yields the homogeneous Poisson point process (HPPP), with intensity λ , and mean measure $\Lambda(B) = \lambda \mu_p(B)$, where $\mu_p(B)$ the volume of B . We write $N \sim IPPP(\Lambda(B))$ to denote this random measure.

The joint distribution of the independent events φ_n , and the number of events $N(\mathcal{W}) = n$ over the window \mathcal{W} , is given by

$$f_N(\varphi_n, n) = \frac{e^{-\Lambda(\mathcal{W})}}{n!} \prod_{i=1}^n \lambda(\mathbf{x}_i) = \frac{1}{n!} e^{-\int_{\mathcal{W}} \lambda(\mathbf{x}) \mu_p(d\mathbf{x})} \prod_{i=1}^n \lambda(\mathbf{x}_i), \quad (7)$$

$n \in \mathbb{N}$. Note that the intensity function uniquely determines the IPPP, where $\lambda(\mathbf{x}) \mu_p(d\mathbf{x})$ assumes the interpretation of the probability of finding a point in an infinitesimal ball of volume $\mu_p(d\mathbf{x})$ centered at \mathbf{x} .

Clearly, in order to describe the point process, one needs to model its intensity $\lambda(\mathbf{x})$, where the integral in Equation (6) is typically not available in closed form, requiring numerical approximations, which in turn introduces a computational burden. The standard approximation is via a Riemann sum; we grid the window \mathcal{W} into L fine, equal-sized cells, each with area A_l , and label the centers of these cells as $\{\mathbf{u}_l : l = 1, 2, \dots, L\}$. Then we can approximate the integral using its Riemann sum

$$\Lambda(\mathcal{W}) = E[N(\mathcal{W})] = \int_{\mathcal{W}} \lambda(\mathbf{x}) \mu_p(d\mathbf{x}) \simeq \sum_{l=1}^L A_l \lambda(\mathbf{u}_l). \quad (8)$$

Alternatively, we can use Monte Carlo integration; let $\mathbf{x}_l \sim \text{Unif}(\mu_p(\mathcal{W}))$, $l = 1, 2, \dots, L$, independent, uniformly drawn points over \mathcal{W} , and write

$$\Lambda(\mathcal{W}) = \int_{\mathcal{W}} \lambda(\mathbf{x}) \mu_p(d\mathbf{x}) = \mu_p(\mathcal{W}) \int_{\mathcal{W}} \lambda(\mathbf{x}) \frac{1}{\mu_p(\mathcal{W})} \mu_p(d\mathbf{x}) \simeq \frac{\mu_p(\mathcal{W})}{L} \sum_{l=1}^L \lambda(\mathbf{x}_l),$$

where the Law of Large Numbers guarantees

$$\frac{\mu_p(\mathcal{W})}{L} \sum_{l=1}^L \lambda(\mathbf{x}_l) \xrightarrow{a.s.} \Lambda(\mathcal{W}), \quad (9)$$

as $L \rightarrow \infty$.

An exact method is obtained if we can write $\lambda(\mathbf{x}) = \lambda g(\mathbf{x})$, where g is a proper density over \mathcal{W} , and $\lambda > 0$, some constant. Then we can rewrite Equation (6) as

$$\Lambda(\mathcal{W}) = \int_{\mathcal{W}} \lambda g(\mathbf{x}) \mu_p(d\mathbf{x}) = \lambda \int_{\mathcal{W}} g(\mathbf{x}) \mu_p(d\mathbf{x}) = \lambda,$$

and therefore λ is a constant describing the average number of events over the region \mathcal{W} , and approximation of the integral is no longer required. More details on this construction for the intensity function can be found in [9], [32], [33] and [34]. Next, we construct a specific IPPP to help us find the zeroes of a given function.

2.2 Zeroes via Poisson point processes

In order to describe the zeroes of $f \in \mathcal{F}_{\mathbb{M}^p}^{\text{MP}}$, we entertain an IPPP model for the random counting measure N_f . Then, point patterns (realizations) from the IPPP N_f will provide realizations of the locations of the zeroes. All we have to work with, is the function f , which satisfies the following mild conditions:

- a) f is known in closed form or can be calculated/approximated well for any $\mathbf{x} \in \mathbb{M}^p$,
- b) f has a finite number of zeroes over a bounded set \mathcal{W} , i.e., $N_f(\mathcal{W}) < \infty$,
- c) f is continuous over a bounded set \mathcal{W} , and
- d) there does not exist a point $\mathbf{y} \in \mathbb{M}^p$, and radius $r > 0$, such that $f(\mathbf{x}) = 0$, for all \mathbf{x} in the open ball $b(\mathbf{y}, r)$.

The latter condition is imposed in order to avoid degenerate or uninteresting cases, e.g., when f vanishes over a given interval, or it oscillates between two values as \mathbf{x} is rational or irrational, and so forth. However, as we will see in our examples in Section 3 the proposed

PPZ algorithm will be able to recover zeroes even in these cases, but the justification is heuristic, since the random measures are locally finite, i.e., we cannot have $N_f(\mathcal{W}) = \infty$.

By definition, the zeroes satisfy $f(\mathbf{x}) = 0$, $\mathbf{x} \in \Xi_f$, so that in terms of an IPPP describing the random measure N_f that would yield a point pattern involving points from the zeroes set Ξ_f , we must have an intensity function that vanishes over all $\mathbf{x} \in \mathcal{W}$, when $f(\mathbf{x}) \neq 0$. Consequently, a natural choice is to consider the IPPP N_f with intensity function

$$\lambda_K(\mathbf{x}) = \exp \{ -K|f(\mathbf{x})|^Q \}, \quad (10)$$

where $K, Q > 0$, and $|\cdot|$ denotes absolute value of a real number when $\mathbb{M} = \mathfrak{R}$ or modulus of a complex number when $\mathbb{M} = \mathbb{C}$. An appropriate norm must be employed when we depart from these standard spaces.

Let us connect the intensity function λ_K of the random measure N_f with the set of distinct zeroes Ξ_f ; rewrite Equation (10) as

$$\lambda_K(\mathbf{x}) = \exp \{ -K|f(\mathbf{x})|^Q \} I(\mathbf{x} \notin \Xi_f) + e^{-K \cdot 0} I(\mathbf{x} \in \Xi_f),$$

and since

$$I(\mathbf{x} \in \Xi_f) = \sum_{\xi \in \Xi_f} \delta_{\xi}(\mathbf{x}),$$

where $\delta_{\xi}(\mathbf{x})$ is Dirac measure (point masses at the zeroes), we have

$$\lambda_K(\mathbf{x}) = \exp \{ -K|f(\mathbf{x})|^Q \} I(\mathbf{x} \notin \Xi_f) + \sum_{\xi \in \Xi_f} \delta_{\xi}(\mathbf{x}). \quad (11)$$

Trivially, as $K \rightarrow +\infty$, the intensity of the IPPP N_f satisfies

$$\lambda_K(\mathbf{x}) \rightarrow \sum_{\xi \in \Xi_f} \delta_{\xi}(\mathbf{x}), \quad (12)$$

pointwise, for all $\mathbf{x} \in \mathcal{W}$. Therefore, we can write

$$\lambda_{\Xi_f}(\mathbf{x}) = \sum_{\xi \in \Xi_f} \delta_{\xi}(\mathbf{x}), \quad (13)$$

to represent the intensity function of the limiting IPPP with realization being a subset of the fixed set Ξ_f . The IPPP with intensity function $\lambda_{\Xi_f}(\mathbf{x})$, will be called the Poisson Point Process of Zeroes (PPPZ).

Naturally, we would like to find the expected number of zeroes over an observation window \mathcal{W} . Owing to the point process theory context we employed, this number is obtained immediately via the intensity measure, i.e., we have

$$E[N_f(\mathcal{W})] = \Lambda_{N_f}(\mathcal{W}) = \int_{\mathcal{W}} \lambda_K(\mathbf{x}) \mu_p(d\mathbf{x}) = \int_{\mathcal{W}} \exp \{ -K|f(\mathbf{x})|^Q \} \mu_p(d\mathbf{x}) < +\infty,$$

and using Equation (11), we can write the latter as

$$\begin{aligned} E [N_f(\mathcal{W})] &= \int_{\mathcal{W}} \exp \{-K|f(\mathbf{x})|^Q\} I(\mathbf{x} \notin \Xi_f) \mu_p(d\mathbf{x}) + \int_{\mathcal{W}} \sum_{\xi \in \Xi_f} \delta_{\xi}(\mathbf{x}) \mu_p(d\mathbf{x}) \\ &= \int_{\mathcal{W} \cap \Xi_f^c} \exp \{-K|f(\mathbf{x})|^Q\} \mu_p(d\mathbf{x}) + \sum_{\xi \in \Xi_f} I(\xi \in \mathcal{W}), \end{aligned}$$

and therefore

$$E [N_f(\mathcal{W})] = \int_{\mathcal{W} \cap \Xi_f^c} \exp \{-K|f(\mathbf{x})|^Q\} \mu_p(d\mathbf{x}) + \#(\Xi_f \cap \mathcal{W}). \quad (14)$$

Consequently, as $K \rightarrow \infty$, using bounded convergence theorem above to swap the order of the limit and integration, leads to

$$E [N_f(\mathcal{W})] \rightarrow \#(\Xi_f \cap \mathcal{W}), \quad (15)$$

as anticipated.

Finally, in terms of the joint distribution of the number of zeroes $N_f(\mathcal{W}) = \#(N_f \cap \mathcal{W})$ and their locations $\varphi_n = \{\mathbf{x}_1, \dots, \mathbf{x}_n\}$, Equation (7) yields

$$\begin{aligned} f_{N_f}(\varphi_n, n) &= \frac{1}{n!} e^{-\Lambda_{N_f}(\mathcal{W})} \prod_{i=1}^n \lambda_K(\mathbf{x}_i) = \frac{1}{n!} e^{-\int_{\mathcal{W} \cap \Xi_f^c} \exp\{-K|f(\mathbf{x})|^Q\} \mu_p(d\mathbf{x}) - \sum_{\xi \in \Xi_f} I(\xi \in \mathcal{W})} \\ &\quad \prod_{i=1}^n \left[\exp \{-K|f(\mathbf{x}_i)|^Q\} I(\mathbf{x}_i \notin \Xi_f) + \sum_{\xi \in \Xi_f} \delta_{\xi}(\mathbf{x}_i) \right], \end{aligned}$$

so that asymptotically, as $K \rightarrow +\infty$, the joint distribution of the number and locations of the IPPP N_f has limit given by

$$f_{N_f}(\varphi_n, n) \rightarrow \frac{1}{n!} e^{-\sum_{\xi \in \Xi_f} I(\xi \in \mathcal{W})} \prod_{i=1}^n \left[\sum_{\xi \in \Xi_f} \delta_{\xi}(\mathbf{x}_i) \right],$$

which is the joint distribution for the PPPZ. Next we discuss special cases and generalizations of the new method for finding zeroes.

2.3 Identifying Extrema and Generalizations

First we note that the set of zeroes Ξ_f of a function f coincides with the set over which the anti-derivative of f , say $g(x) = \int f(x) d\mu_1(x)$, with $f = g'$, achieves all of its its extrema (minima and maxima) in \mathcal{W} . In other words, in order to find extrema of the function g we need to find the zeroes of its derivative f . More precisely, assume we wish to find the set where the extrema of $g : \mathbb{M} \rightarrow \mathbb{M}$ are obtained, i.e.,

$$E_g = \{\xi \in M : g(x) \leq g(\xi) \text{ or } g(\xi) \leq g(x), \text{ for all } x \text{ in a neighborhood of } \xi \in \mathbb{M}\}.$$

If the derivative $\frac{d}{dx}g(x) = g'(x) = f(x)$ is available in closed form, then the extrema of g are obtained at the zeros Ξ_f of f . For multivariate functions $g : \mathbb{M}^p \rightarrow \mathbb{M}$, if we have the gradient $\nabla g(\mathbf{x}) = \left[\frac{\partial}{\partial x_1} g(\mathbf{x}), \dots, \frac{\partial}{\partial x_p} g(\mathbf{x}) \right]$ in closed form, we can use the PPPZ method for finding zeroes of the gradient function as we see next.

More generally, assume that we wish to find the set of zeroes of a multivariate, vector valued function $\mathbf{f} : \mathbb{M}^p \rightarrow \mathbb{M}^q$, $p, q \in \mathbb{N}^+ = \{1, 2, 3, \dots\}$, with

$$\mathbf{f}(\mathbf{x}) = [f_1(\mathbf{x}), \dots, f_q(\mathbf{x})],$$

for all $\mathbf{x} \in \mathbb{M}^p$. Now define the one dimensional function of \mathbf{x} based on \mathbf{f} given by

$$\|\mathbf{f}(\mathbf{x})\| = \sum_{i=1}^q |f_i(\mathbf{x})|,$$

so that $\boldsymbol{\xi} \in \Xi_{\mathbf{f}} = \{\mathbf{x} \in \mathbb{M}^p : \mathbf{f}(\mathbf{x}) = \mathbf{0}\}$, if and only if $\|\mathbf{f}(\boldsymbol{\xi})\| = 0$. Therefore, the PPPZ can be applied to the modification of the intensity (10) given by

$$\lambda_K(\mathbf{x}) = \exp \left\{ -K \left| \sum_{i=1}^q |f_i(\mathbf{x})| \right|^Q \right\}, \quad (16)$$

and it will provide the zeroes set $\Xi_{\mathbf{f}}$ of \mathbf{f} .

When we wish to find all the points of extrema, i.e., local and global minima and maxima, but it is hard to obtain the partial derivatives of f in closed form to look for its zeroes, we consider finding the zeroes of the approximation of the derivative of f given by

$$\widehat{\frac{df(x)}{dx}} = \frac{f(x + \varepsilon) - f(x)}{\varepsilon}, \quad (17)$$

where ε is very small. Similarly, in the multivariate case, we use

$$\widehat{\frac{\partial f(\mathbf{x})}{\partial x_i}} = \frac{f_i(\mathbf{x}) - f(\mathbf{x})}{\varepsilon}, \quad (18)$$

where

$$f_i(\mathbf{x}) = f(x_1, \dots, x_{i-1}, x_i + \varepsilon, x_{i+1}, \dots, x_p), \quad (19)$$

for each $i = 1, 2, \dots, p$. In order to find the extrema of f we use $\widehat{\nabla f(\mathbf{x})} = \left[\widehat{\frac{\partial f(\mathbf{x})}{\partial x_1}}, \dots, \widehat{\frac{\partial f(\mathbf{x})}{\partial x_p}} \right]$ to approximate $\nabla f(\mathbf{x})$ and then apply the PPPZ with intensity function of Equation (16), i.e., we take

$$\lambda_K(\mathbf{x}) = \exp \left\{ -K \left| \sum_{i=1}^p \left| \widehat{\frac{\partial f(\mathbf{x})}{\partial x_i}} \right| \right|^Q \right\}, \quad (20)$$

in order to find the solutions of $\nabla f(\mathbf{x}) = \mathbf{0}$.

Finally, for any optimization problem or the PPPZs above, we can easily add any constraints we wish directly to the intensity function. More precisely, a constraint is described

as a subset \mathcal{C} of \mathcal{X} , e.g., $\mathcal{C} = \left\{ \mathbf{x} : \sum_{i=1}^p x_i \geq 1 \right\}$, and it simply alters the window of observation, i.e., we use the PPPZ with intensity function $\lambda_K(\mathbf{x})I(\mathbf{x} \in \mathcal{C})$ over the window $\mathcal{W} \subset \mathcal{X}$, where $I(\cdot)$ denotes the indicator function.

We discuss the implementation details of the PPPZ, along with many illustrative examples, in the next section.

3 Implementation and Examples

The theoretical justification of the PPPZ method is straightforward and intuitively appealing, however, in practice, since the computers cannot handle infinity and even super computers overflow easily, we will have to be very careful with the implementation of the proposed method. Specifically, since we cannot perform a fine enough grid search to check for a zero of f (and we do not want to do that anyways), we will have to produce a simulation method to approximate zeroes that is a) as fast as possible, b) accurate (up to our liking), and c) flexible enough to be amenable to changes.

In particular, the PPPZ as constructed depends on the constants $K > 0$ and $Q > 0$, which control how fast we will reject potential zeroes, as well as, a required tolerance variable Tol that will act as the cutoff value for what is an acceptable zero, i.e., when $|f(\mathbf{x})| < Tol$, we will treat \mathbf{x} as a zero of f . For example, setting $Tol = 10^{-500}$ will never be easy to achieve in a reasonable amount of time and without introducing overflows or memory allocation problems in the computer, or long running times, even for easy, one dimensional functions. Instead, we will provide a main simulation method to approximate the zero set Ξ_f for a specific starting Tol_{start} , and then if one wishes to get closer and closer to the zero, we will propose an adaptive simulation method that can take us to a reasonable target tolerance $Tol_{end} < Tol_{start}$, e.g., $Tol_{end} = 10^{-10}$, before overflows occur in the computer. Moreover, as we will see, the adaptive simulation method can take a lot of time to run for $Tol_{end} < 10^{-20}$, depending on the function under consideration and the chosen values for parameters K and Q .

Recall that $|\cdot|$ is used as shorthand for the absolute value for real f , and complex modulus for complex f . In view of Equation (10), as the constant $Q > 1$ becomes larger, values of $|f(\mathbf{x})|$ that are less than 1 become smaller and smaller, so that larger Q brings values of $|f(\mathbf{x})| < 1$ closer to zero even if there is no zero of f at that point. As a consequence, large Q erroneously suggests that the intensity function λ_K is large at a specific point when it should not, and will lead to a realization of the zero set Ξ_f that may include non-zeroes of the function f . On the other hand, as $Q < 1$ becomes smaller and smaller, values of $|f(\mathbf{x})| < 1$ become larger and larger, and the intensity once again will erroneously suggest that there is no zero at a certain point even if there is one there.

When $|f(\mathbf{x})| > 1$, the value \mathbf{x} is certainly not a zero of f , and large values of Q correctly increase $|f(\mathbf{x})|^Q$, so that the intensity becomes smaller and this point will not appear in a realization of N_f . For $|f(\mathbf{x})| > 1$, as $Q \rightarrow 0^+$ from the right, leads to $|f(\mathbf{x})|^Q \rightarrow 1^+$, from the right, and even if we have a zero at \mathbf{x} , it will not be retrieved in a realization of N_f , since the intensity will never go to zero.

The above observations suggest that appropriate values for the power should be away

from 0 and not too large, e.g., $0 < Q \leq 2$. Following extensive simulations, it is recommended that the readers use $Q = 0.5$ for real functions and $Q = 2$ for complex functions. As the dimension increases for multivariate real functions, it is best to choose $Q = 1$. We will discuss the effect of $K > 0$ in the next section.

It should be emphasized, that unlike existing methods for finding function zeroes or function optimization, such as simulated annealing or Newton methods and their modifications, the proposed PPPZ can provide all zeroes using a single realization of the model (one iteration). Furthermore, the method does not require the construction of a stochastic process that converges to a zero or point of extrema, and neither requires forms for the derivative of the function or iterations in order to obtain a zero. That means the PPPZ does not suffer from any of the problems such methods are notorious for; e.g., getting locked in local maxima or not achieving convergence.

3.1 Algorithm for finding zeroes

Simulating a HPPP N with intensity $\lambda > 0$ over a bounded set (window) \mathcal{W} is accomplished via conditioning, that is

- (i) simulate the number of points $N(\mathcal{W}) \sim Pois(\lambda\mu_p(\mathcal{W}))$, say $N(\mathcal{W}) = n$, and then
- (ii) simulate n points as an independent random sample from the uniform distribution over \mathcal{W} .

In order to simulate the IPPP N_f with intensity function of Equation (10), over a bounded set \mathcal{X} , we use a modification of the standard thinning (rejection) sampler (see [31]). The following algorithm, and its adaptive version, were written in R, incorporating faster C++ code via the RCPP and RcppArmadillo packages, and are available to the scientific community, currently at this [website](#).

Algorithm 1 (Poisson Point Process Zeroes) *Consider the IPPP $N_f \sim IPPP(\lambda_K(\cdot))$, and note that for any given real $Q, K > 0$, integer $N > 1$ and any window $\mathcal{W} \subset \mathcal{X} \subset \mathbb{M}^p$, we have*

$$\sup_{\mathbf{x} \in \mathcal{W}} \lambda_K(\mathbf{x}) = \sup_{\mathbf{x} \in \mathcal{W}} \exp \{ -K|f(\mathbf{x})|^Q \} \leq 1 < N.$$

1. *Select a target tolerance $Tol > 0$; points $\mathbf{x} \in \mathcal{W}$, with $|f(\mathbf{x})| < Tol$, are considered to be zeroes of f . Note that if this value is too small, it is possible that none of the zeroes will be identified from any realizations of N_f , nomatter that the values of N or K .*
2. *Simulate a HPPP($N\mu_p(\mathcal{W})$) over \mathcal{W} , say $\varphi_n = \{\mathbf{x}_1, \dots, \mathbf{x}_n\}$. Clearly, the larger the N , the better the exploration of the window \mathcal{W} , but we do not want to perform a grid search, and therefore, N will be set to $1000p$ or less, where p is the dimension of the event space \mathbb{M}^p .*
3. *Independently retain each point $\mathbf{x}_i \in \mathcal{W}$, with probability $\lambda_K(\mathbf{x}_i)$, i.e., generate $U \sim Unif(0, 1)$, and retain the point if*

$$U < \exp \{ -K|f(\mathbf{x}_i)|^Q \}. \tag{21}$$

4. The realization of $N_f \sim IPPP(\lambda_K(\cdot))$, consists of the retained events, and is treated as an approximation of the set Ξ_f .

Regarding the selection of $K > 0$, and its effect in practice; although the theory presented tells us that we must have $K \rightarrow \infty$, in reality we cannot choose K too large, since the checks required in Equation (21) will fail even at points that are zeroes within the given Tol value. As K increases, the intensity will become smaller and smaller even at points that are not the function zeroes, which leads to erroneously identifying zeroes for the specific Tol value. Even if \mathbf{x}_i is near a zero, with $|f(\mathbf{x}_i)| < Tol$, large K values will erroneously reject this point from the realization of N_f . On the other hand, as K decreases, the intensity increases and the algorithm will once again erroneously propose realizations that are non-zeroes of f . Therefore, in practice we need to use a relatively small K , e.g., values $K = 10, 20$ or 50 , seem to work best in simulated examples. Setting $K = 100$, or larger, one encounters a situation where only part of the set Ξ_f appears in a realization of N_f , that is, only part of the set of zeroes are recovered.

Instead of guessing the best values of N , K and Q , that will give us all the zeroes set Ξ_f in the realization of N_f , and in order to achieve a specific given Tol value for all zeroes in Algorithm 1, we consider the following modifications.

Remark 2 (Adaptive PPPZ algorithm) *We discuss an adaptive version of Algorithm 1, and the modification of each one of its steps, in order to achieve a desired Tol_{end} . In the adaptive PPPZ (APPPZ) version, the reader can choose a number of iterations, $Iter \geq 1$. Without loss of generality, assume $p = 1$, and consider the zeroes of f over the window $\mathcal{W}_{1,1} = [x_{min}, x_{max}]$.*

1. The adaptive version of the algorithm, allows for a large starting tolerance and a very small end tolerance. In particular, it is recommended that the reader sets $Tol_{start} = 10^{-1}$ and $Tol_{end} = 10^{-10}$. The current tolerance Tol_{cur} is set to Tol_{start} .
2. The point pattern φ_n generated at this step can be thought of as the starting value of the adaptive sampling algorithm.
3. The adaptive version of steps 3 and 4, looks first for zeroes within the current tolerance. In order to achieve the specific tolerance Tol_{cur} , we retain a point if

$$U < \exp \left\{ -K |f(\mathbf{x}_i)|^Q \right\} I(|f(\mathbf{x}_i)| < Tol_{cur}), \quad (22)$$

where $I(\cdot)$ denotes the indicator function.

For the first iteration only, if no zeroes are found in the realization of N_f , the current tolerance is increased by $10Tol_{cur}$, the number of points is increased by $10N$, and we go back to step 1.

Assume that we find $\varphi_{Iter, n_1} = \{x_1, \dots, x_{n_{Iter}}\}$ potential zeroes within Tol_{cur} . We build smaller windows centered at each of the potential zeroes, $\mathcal{W}_{Iter, j} = [x_j - r, x_j + r]$, $j = 1, 2, \dots, n_{Iter}$, where r is 1% of the (parent) window \mathcal{W} , reduce the current tolerance by 10%, i.e., the next iteration tolerance is $Tol_{cur}/10$, and go back to step 1 for each window identified. Note that increasing r (up to 50%) will provide a better exploration

about the zero x_j at the cost of computational speed.

When $Iter > 1$, if no zeroes are found for the current window and given Tol_{cur} , the window is slightly increased by setting $1.1r$, the number of points is increased by $1.1N$, and we generate a new realization of N_f over the new window, until we get a zero within this tolerance level.

This procedure is guaranteed to refine the values where the zeroes are obtained for the current tolerance. The more the iterations, the closer to the end tolerance we entertain the zeroes will be, but the procedure becomes very slow as the tolerance becomes smaller. Further note that since each sub-window $\mathcal{W}_{Iter,j}$ can yield many realizations for a specific zero within Tol_{cur} , e.g., say two zeroes at 1.0001 and 1.0002, a post processing effect is applied, where we keep only the zero with the smallest $|f(\mathbf{x})|$ for all zeroes identified within the window $\mathcal{W}_{Iter,j}$.

4. When the maximum number of iterations is reached or $Tol_{cur} < Tol_{end}$, the adaptive algorithm stops and the zeroes within Tol_{cur} are retrieved.

Note that it is possible that the function f does not have any zeroes over a given window. This case corresponds to none of the generated points being valid zeroes, i.e., satisfying $|f(\mathbf{x})| < Tol_{end}$, and it is captured by the algorithm when a window yields no acceptable zeroes. In this case, the window "dies" out and is removed from further consideration.

The point process created by the adaptive algorithm of Remark 2, is mathematically equivalent to a Neyman-Scott process (for 2 iterations), where the parent process is the IPPP N_f with intensity function $\lambda_K(\cdot)$ of Equation (10), the parents are removed, and in every window a child point process is generated as an IPPP with intensity function $\lambda_K(\cdot)$, independently. The Neyman-Scott process consists of the superposition of all offspring points.

For higher number of iterations we generalize the Neyman-Scott process, and continue the following way; using the first level offspring as the parent process, we generate the child processes at each window and obtain the second level offspring point process as the superposition of all the generated child processes. Proceed in a similar manner for any number of iterations to obtain a finer and finer collection of offspring points, that can get as close as we want to the zeroes of f . When Tol_{end} is extremely small and the number of windows increases, we encounter three major drawbacks; computational speed, computer overflows and memory allocation problems. Some illustrative examples are definitely in order.

3.2 Examples: one dimensional real functions

In the examples that follow we set $N = 1000$, $K = 10$, $Q = 0.5$, $Tol_{start} = 10^{-1}$ and $Tol_{end} = 10^{-15}$. We begin with some simple examples in order to appreciate the behavior of the PPPZ and Algorithm 1, along with its modification of Remark 2.

Consider the function $f(x) = \cos(x)$, with derivative $f'(x) = -\sin(x)$, over the window $\mathcal{W} = [-15, 15]$. We run the APPPZ algorithm (for 1, 5 and 10 iterations), and present the results in Table 1 and Figure 1 (left plot, using results for 10 iterations). The derivative is displayed in green and the intensity function is displayed in blue color. The locations

where the zeros are obtained are displayed as red points. Note that the zeroes of $\cos(x)$ are the values where the extrema for the function $-\sin(x)$ are attained. The zero values are presented in Table 1, where we can observe the effect of the tolerance variable and the number of iterations, as well as the time the PPPZ was run in each case.

We also run the APPPZ (10 iterations, 0.68s) on the derivative of $\cos(x)$ over $\mathcal{W} = [-15, 15]$, in order to find the points of extrema. Figure 1 (right) presents the results where we found the 9 points of extrema (zeroes of the derivative), with the global maximum being 1 attained at $x = -12.56637, -6.283185, 2.200653e - 11, 6.283185, 12.56637$, and the global minimum is -1 attained at $x = -9.424778, -3.141593, 3.141593, 9.424778$.

Now consider the function $f(x) = \sin(x/20) + \cos^2(x)$, displayed in Figure 2 (left). This is a more interesting function with a lot of different local maxima and local minima. We run the APPPZ for 10 iterations (3.74s) and obtained 9 zeroes displayed in Table 2 (left). We also run the APPPZ (5 iterations, 0.32s) on the derivative of $\sin(x/20) + \cos^2(x)$ in order to find the points of extrema, with the results presented in Table 2 (right) and in Figure 2 (right). We obtained 19 points of extrema with global maximum 1.588194 at $x = 12.58658$, and global minimum -0.6498092 at $x = -14.15617$.

For comparison purposes, we used the `optim R` function in an attempt to replicate the optimization above; the results using the simulated annealing method were not surprising (with starting value at the point 0), since the algorithm kept getting locked into local maxima. To be fair, this function is a very hard situation for the simulated annealing approach when it comes to function maximization. Regardless, all existing methods in the literature, even if they manage to provide a zero of the target function, they do not provide the whole set of zeroes like the PPPZ approach, which is one of the main advantages of the proposed method.

Now consider the APPPZ algorithm over $\mathcal{W} = [0, 5]$ for the function $f(x) = 35(x - 3)^5(x - 2)^{10}$, displayed in Figure 3 in black color. We run the algorithm for 10 iterations in two cases with the left plot (55.14s) showing the true zeroes at $x = 2, 3$, and the right plot (61.01s) illustrating what can happen when the function is very close to zero for a range of its values; for the given tolerance $Tol = 10^{-10}$, the adaptive algorithm ends up proposing three zeroes. In particular, the two zeroes on the left plot correspond to $x = 1.999900944$ with $f(x) = -3.184907493e - 39$, and $x = 2.999829027$ with $f(x) = -5.104621074e - 18$, while the three zeroes in the right plot are obtained for $x = 1.933949874$ with $f(x) = -7.615398755e - 11$, $x = 1.999994981$ with $f(x) = -3.553477504e - 52$, and $x = 3.000340727$ with $f(x) = 1.612789525e - 16$. In such cases where the function is very close to zero for a lot of values, the best approach is to lower the tolerance and rerun the algorithm multiple times.

3.3 Examples: one dimensional complex functions

For the following examples we will assume that $p = 1$ and $\mathbb{M} = \mathbb{C}$, the complex plane, and investigate classic complex-valued functions such as polynomials with complex coefficients and Riemann's ζ function. In what follows, for any $s = \sigma + it \in \mathbb{C}$, we let $|s| = \sqrt{s\bar{s}} = \sqrt{\sigma^2 + t^2}$ denote complex modulus, where $\bar{s} = \sigma - it \in \mathbb{C}$, the complex conjugate.

1 Iteration, 0.13s	$Tol = 0.1$	5 Iterations, 0.18s	$Tol = 1e - 05$	10 Iterations, 0.49s	$Tol = 1e - 10$
x	$f(x)$	x	$f(x)$	x	$f(x)$
-14.137392144	-2.252030286e-04	-14.137166819	1.225845155e-07	-14.137166941	-1.093647799e-11
-10.995832121	2.578329669e-04	-10.995573397	-8.904471795e-07	-10.995574288	-1.534992806e-11
-7.854048223	-6.658926018e-05	-7.853984927	-3.292605847e-06	-7.853981634	-8.302128345e-11
-4.713078998	6.900175898e-04	-4.712390497	1.516723439e-06	-4.712388980	3.162873801e-11
-1.570671543	1.247837813e-04	-1.570794105	2.22225828e-06	-1.570796327	2.152972817e-11
1.571162785	-3.664586003e-04	1.570800172	-3.844757923e-06	1.570796327	-4.959004857e-11
4.713414288	1.025307562e-03	4.712387831	-1.148976112e-06	4.712388980	4.585380358e-11
7.854884625	-9.029913153e-04	7.853985505	-3.870612018e-06	7.853981634	-1.200786608e-11
10.993944642	-1.629645175e-03	10.995574324	3.635807168e-08	10.995574288	4.851187667e-11
14.134706296	2.460642644e-03	14.137167606	-6.651373473e-07	14.137166941	-1.299527556e-11

Table 1: The APPPZ algorithm for the function $f(x) = \cos(x)$, after 1 iteration (left), 5 iterations (middle) and 10 iterations (right). Note that we can get as close as we want to the zero, although even a single realization (iteration) provides a good approximation to the zeroes set Ξ_f .

APPPZ zeroes, 3.74s, $Tol = 1e - 10$, $x(f(x))$
-13.236196796(7.433831328e-11), -11.839087124(-2.269140431e-11), -10.221080134(-9.227130171e-11), -8.553728223(-5.538963732e-11), -7.217681823(1.911387715e-11), -5.246703175(-2.103101027e-11), -4.236080310(5.839356776e-12), -1.882374611(-2.198349836e-11), -1.311891013(1.582591003e-11)
APPPZ extrema, 0.32s, $Tol = 1e - 05$, $x(f'(x))$
-14.15616540(1.755263e-06), -12.54612646(3.221867e-06), -11.01688533(-4.938272e-06), -9.40247893(-7.771561e-06), -7.87707455(2.540745e-06), -6.25938774(-6.095124e-06), -4.73670165(-1.800227e-06), -3.11689054(9.805490e-06), -1.59573098(-7.598505e-06), 0.02500947(1.765255e-06), 1.54585904(-3.081008e-06), 3.16628790(4.198863e-06), 4.68806496(3.904654e-06), 6.30696349(-4.112266e-06), 7.83086437(-1.901257e-06), 9.44704644(2.697842e-06), 10.97423862(1.572076e-06), 12.58658194(9.379164e-06), 14.11814154(9.655610e-06)

Table 2: The APPPZ algorithm for the function $f(x) = \sin(x/20) + \cos^2(x)$, to obtain the 9 function zeroes (10 iterations, top), and the APPPZ for its derivative to obtain the 19 points of extrema (5 iterations, bottom).

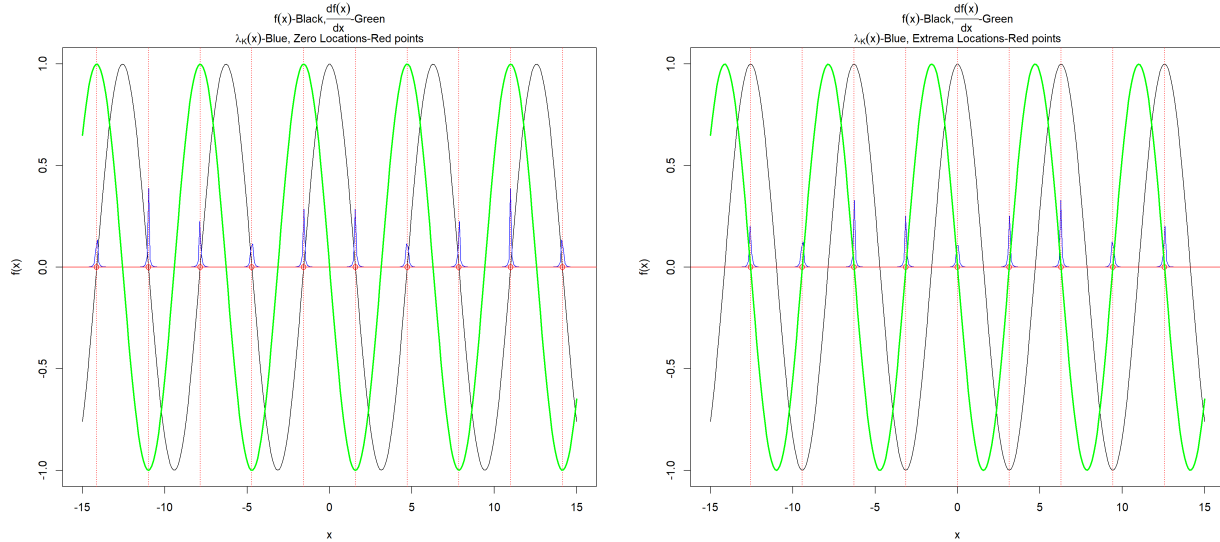


Figure 1: The APPPZ algorithm over $\mathcal{W} = [-15, 15]$ for the function $f(x) = \cos(x)$ (black color). We run the algorithm for 1, 5, and 10 iterations, with the latter displayed (left plot). The derivative $f'(x) = -\sin(x)$ is displayed in green and the intensity function is displayed in blue color. The zeroes are displayed as red points. Note that the zeroes of $\cos(x)$ are the values where the extrema for the function $-\sin(x)$ are attained. The zeroes are presented in Table 1. The right plot presents the results of the PPPZ on the zeroes of the derivative (i.e., the points of extrema of $\cos(x)$).

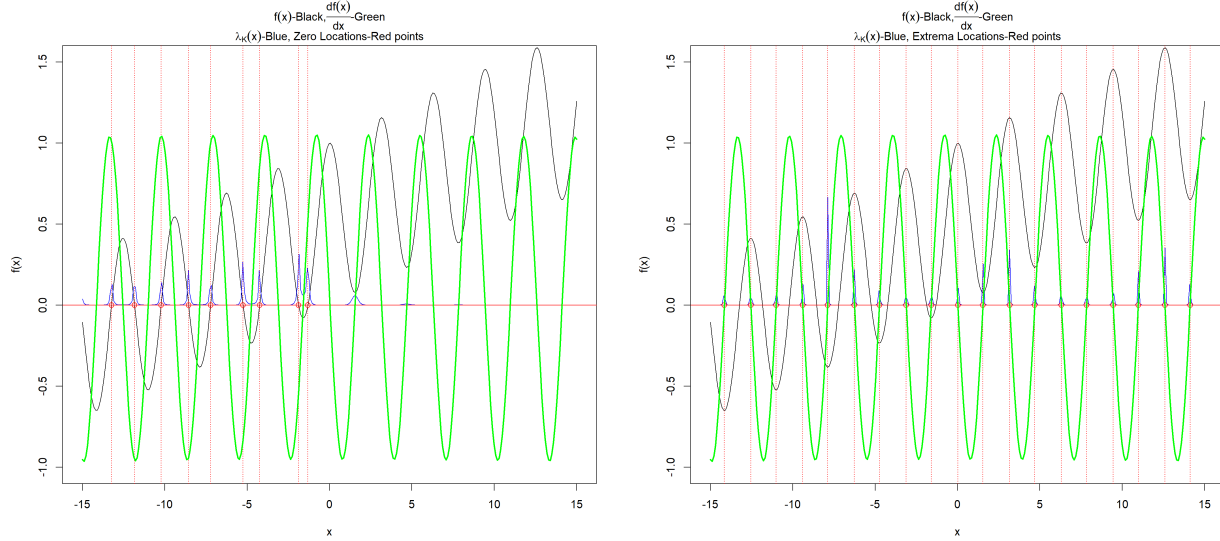


Figure 2: The AAPPZ algorithm over $\mathcal{W} = [-15, 15]$ for the function $f(x) = \sin(x/20) + \cos^2(x)$ (left plot in black color, algorithm was run for 10 iterations). The right plot presents the results of the PPPZ on the zeroes of the derivative (i.e., the points of extrema of $\sin(x/20) + \cos^2(x)$). The derivative is displayed in green and the intensity function is displayed in blue color. The zeros are displayed as red points.

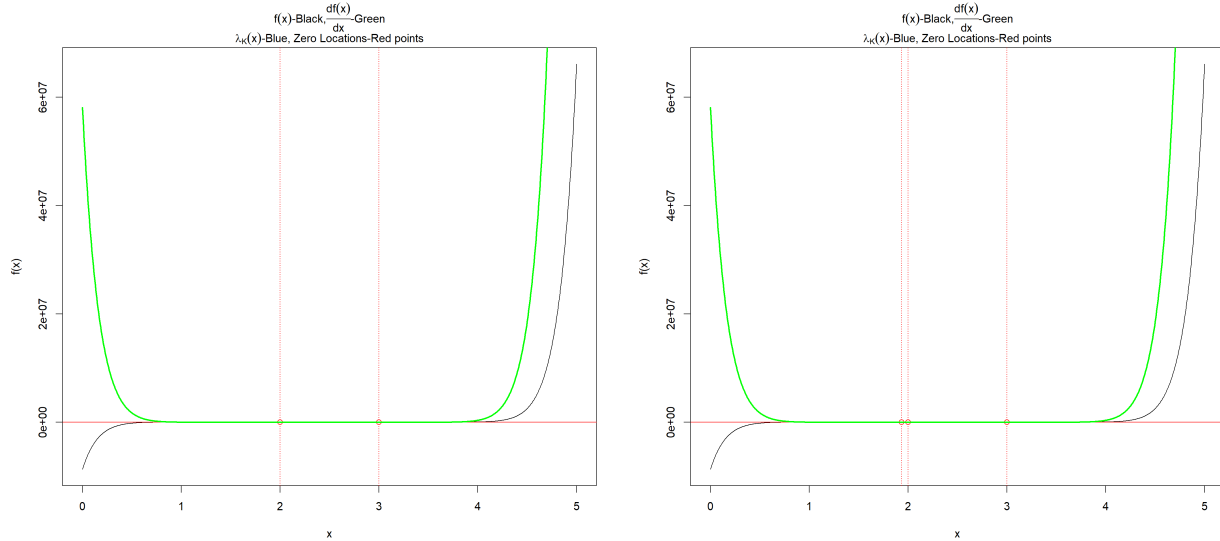


Figure 3: The AAPPZ algorithm over $\mathcal{W} = [0, 5]$ for the function $f(x) = 35(x-3)^5(x-2)^{10}$, in black color. We run the algorithm for 10 iterations in two cases with the left plot showing the true zeroes at $x = 2, 3$, and the right plot illustrating what can happen when the function is very close to zero for a range of its values; for the given tolerance $Tol = 1e - 10$, the adaptive algorithm ends up proposing three zeroes. The derivative is displayed in green and the intensity function is displayed in blue color. The zeros are displayed as red points.

3.3.1 Complex polynomials

Define the complex polynomial $p(s) = (s - 0.5 + 1i)^2(s - 1.0 - 0.5i)^3$, for all $s = \sigma + it \in \mathbb{C}$, with two roots at $s = 0.5 - 1i$ and $s = 1 + 0.5i$. Consider the APPPZ with $N = 1000$, $K = 15$, $Q = 2$, $Tol_{start} = 10^{-1}$, $Tol_{end} = 10^{-15}$, and intensity of the form

$$\lambda_K(s) = \exp \{-K|p(s)|^Q\} = \exp \{-15(p(s)\bar{p}(s))\}, \quad (23)$$

so that we require the zeroes of the 2-dimensional real function $f(\sigma, t) = f(s) = p(s)\bar{p}(s)$. The APPPZ algorithm was run for 10 iterations (89.21s). We obtain two roots at $s = 0.4999996331 - 1.0000000280i$, with modulus square $f(s) = 5.351451840e - 13$, and $s = 0.999999858 + 0.5000061853i$, with modulus square $f(s) = 5.915964743e - 16$, so that the true roots are recovered very well.

Now consider a complex polynomial $p_n(s) = \prod_{k=1}^n (s - \xi_k)$, where $s, \xi_k \in \mathbb{C}$, and ξ_k are the roots, $s \in \mathcal{W} = \{\sigma + it : -1 < \sigma < 1, -1 < t < 1\} \subset \mathbb{C}$. We randomly generated the roots $\xi_k = \sigma_k + it_k$, $k = 1, 2, \dots, n$, independently, as uniform random variables for their real and imaginary parts, i.e., $\sigma_k, t_k \sim Unif(-1, 1)$. We take $n = 10$ and run the APPPZ (12584.62s) with $N = 10000$, $K = 10$, $Q = 2$, $Tol_{start} = 10^{-1}$, $Tol_{end} = 10^{-15}$, and intensity of the form (23). The roots are displayed in Figure 4 (left), with the true roots denoted by x's (black) and the recovered roots as o's (red). Note that all roots are recovered well except for one (with σ near 0.9); more precisely we have 9 roots at the following locations (with $p(s)\bar{p}(s)$ in parenthesis): $-0.9508137350 - 0.4145544947i$ ($3.134447927e - 07$), $-0.9460540885 + 0.5432386222i$ ($2.211998440e - 06$), $-0.8238205595 + 0.1920549400i$ ($3.662131736e - 07$), $-0.7024684132 - 0.9643830442i$ ($1.636778800e - 06$), $-0.6467435614 - 0.6756187027i$ ($1.572207974e - 07$), $-0.6199301022 + 0.8267882050i$ ($2.843105626e - 06$), $-0.2347544854 - 0.5322633364i$ ($9.451631995e - 08$), $0.3364580270 + 0.1769367759i$ ($4.945290057e - 07$), and $0.4259629178 + 0.3331144697i$ ($1.333234823e - 06$).

3.3.2 Riemann's ζ function

Consider Riemann's ζ function (see [7], [22]) defined for any complex number $s = \sigma + it \in \mathbb{C}$ by

$$\zeta(s) = \sum_{n=1}^{+\infty} \frac{1}{n^s} = \sum_{n=1}^{+\infty} \frac{1}{n^\sigma} n^{-it} = \sum_{n=1}^{+\infty} \frac{1}{n^\sigma} e^{-it \ln n}, \quad (24)$$

where the sum converges if $\sigma > 1$. The ζ function is of paramount importance in number theory, since it provides insight on the distribution of prime numbers. The non-trivial zeroes of ζ are obtained when $s = -2, -4, -6, \dots$, and any other zeroes are called nontrivial zeros.

Riemann's hypothesis states that the real part of every non-trivial zero of the ζ function is 0.5, i.e., the remaining zeroes are obtained on the critical line $0.5 + it$, for some $t \in \mathfrak{R}$. Some of the zeroes include $1/2 \pm 14.134725\dots i$, $1/2 \pm 21.022040\dots i$, $1/2 \pm 25.010858\dots i$, $1/2 \pm 30.424876\dots i$, $1/2 \pm 32.935062\dots i$, $1/2 \pm 37.586178\dots i$, and $1/2 \pm 40.918719\dots i$. Our purpose here is not to prove or disprove the hypothesis, but rather illustrate the PPPZ for this important function and verify some of the zeroes that have been already discovered in the literature.

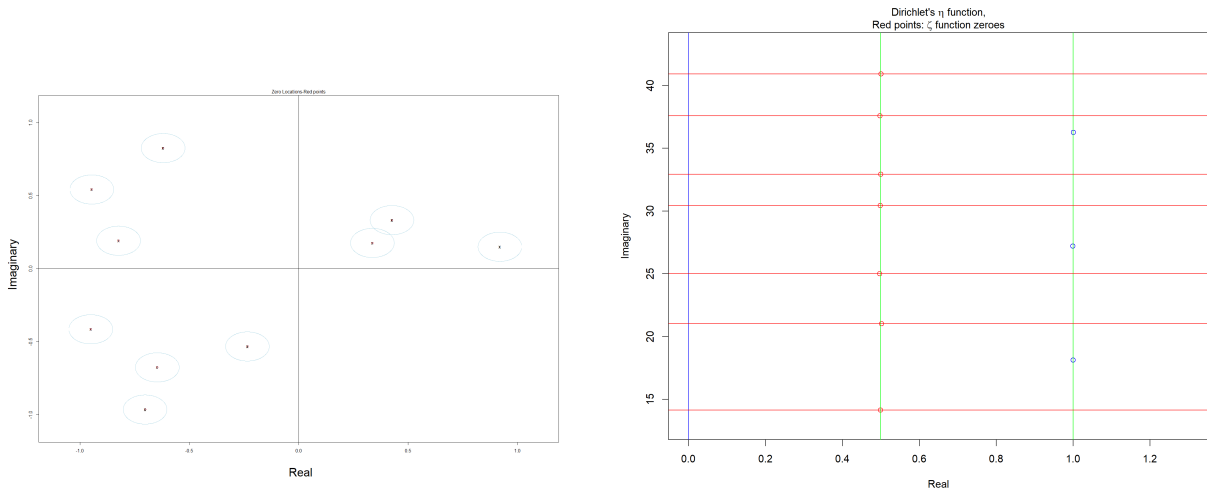


Figure 4: (left) Roots of a complex polynomial $p_{10}(s) = \prod_{k=1}^{10} (s - \xi_k)$, with randomly generated real and imaginary parts of the roots ξ_k , independently, as uniform random variables over $Unif(-1, 1)$. The true roots denoted by x's (black) and the recovered roots as o's (red). Note that all roots are recovered well except for one (with real part near 0.9). (right) The APPPZ algorithm over $\mathcal{W} = \{\sigma + it : 0 < \sigma < 1.3, 13 < t < 43\} \subset \mathbb{C}$ for the η function. The zeros of the ζ function are displayed as red points and the zeroes of the η function on the strip $\sigma = 1$, as green points. The red horizontal lines correspond to the well known zeroes of the strip $\sigma = 0.5$ with imaginary part $t = 14.134725, 21.022040, 25.010858, 30.424876, 32.935062, 37.586178, \text{ and } 40.918719$.

Recall that Dirichlet's η function (also known as the alternating ζ function, see [41], [22]), which converges for all $\sigma > 0$, is defined by

$$\begin{aligned}\eta(s) &= \sum_{n=1}^{+\infty} \frac{(-1)^{n+1}}{n^s} = \sum_{n=1}^{+\infty} \frac{(-1)^{n+1}}{n^\sigma} e^{-it \ln n} \\ &= \left(\sum_{n=1}^{+\infty} \frac{(-1)^{n+1}}{n^\sigma} \cos(t \ln n) \right) - i \left(\sum_{n=1}^{+\infty} \frac{(-1)^{n+1}}{n^\sigma} \sin(t \ln n) \right),\end{aligned}$$

and therefore

$$\eta(s) = \eta_{\text{Re}}(\sigma, t) - i\eta_{\text{Im}}(\sigma, t), \quad (25)$$

where

$$\eta_{\text{Re}}(\sigma, t) = \sum_{n=1}^{+\infty} \frac{(-1)^{n+1}}{n^\sigma} \cos(t \ln n), \quad (26)$$

and

$$\eta_{\text{Im}}(\sigma, t) = \sum_{n=1}^{+\infty} \frac{(-1)^{n+1}}{n^\sigma} \sin(t \ln n). \quad (27)$$

Now note that the alternating form of the ζ function is defined via

$$\zeta(s) = \frac{1}{1 - 2^{1-s}} \sum_{n=1}^{+\infty} \frac{(-1)^{n+1}}{n^s} = \frac{1}{1 - 2^{1-s}} \eta(s), \quad (28)$$

and it is the analytic continuation of (24) for all $\sigma > 0$, except for $\sigma = 1$. Considering the factor $1 - 2^{1-s}$, we note that

$$0 = 1 - 2^{1-s} = 1 - 2^{1-\sigma} \cos(t \log 2) + i2^{1-\sigma} \sin(t \log 2),$$

so that

$$\begin{aligned}1 - 2^{1-\sigma} \cos(t \log 2) = 0 \\ 2^{1-\sigma} \sin(t \log 2) = 0\end{aligned} \Rightarrow \begin{aligned}2^{1-\sigma} \cos(t \log 2) = 1 \\ \sin(t \log 2) = 0\end{aligned},$$

and using the second equation we obtain

$$\sin(t \log 2) = 0 \Rightarrow t = \frac{2k\pi}{\log 2},$$

for all integers $k \neq 0$, and as a result

$$2^{1-\sigma} \cos(t \log 2) = 1 \Rightarrow \sigma = 1,$$

i.e., all zeroes of $1 - 2^{1-s}$ are given by the complex numbers $1 + ik\pi/\log 2$, for all integers $k \neq 0$. Since

$$\eta(s) = (1 - 2^{1-s}) \zeta(s), \quad (29)$$

for $\sigma > 0$, all zeroes of η include $1 + i2k\pi/\log 2$, $k \neq 0$, and all the zeroes of the ζ function. Therefore, assuming that Riemann's hypothesis is correct, all zeroes of η for $0 < \sigma < 1$,

$t > 0$, must be located on the two parallel lines (strips) of the complex plane with $\sigma = 0.5$ and $\sigma = 1$.

Consequently, we consider the PPPZ with intensity function (10) (with $K = 15$, $Q = 2$) of the form

$$\lambda_K(s) = \exp \{-K|\eta(s)|^Q\} = \exp \{-15(\eta(s)\bar{\eta}(s))\}, \quad (30)$$

with $\bar{\eta}$ the conjugate of the function η , and using Equation (25), we have

$$\bar{\eta}(s) = \sum_{n=1}^{+\infty} \frac{(-1)^{n+1}}{n^\sigma} e^{it \ln n} = \eta_{\text{Re}}(\sigma, t) + i\eta_{\text{Im}}(\sigma, t),$$

for all $s \in \mathbb{C}$. Thus we can write the modulus square $|\eta(s)|^2 = \eta(s)\bar{\eta}(s)$ as

$$|\eta(s)|^2 = \eta(s)\bar{\eta}(s) = \eta_{\text{Re}}^2(\sigma, t) + \eta_{\text{Im}}^2(\sigma, t),$$

which is a real function in two dimensions.

We run the APPPZ algorithm over the window $\mathcal{W} = \{\sigma + it : 0 < \sigma < 1.3, 13 < t < 43\} \subset \mathbb{C}$ for the η function with the results displayed in Figure 4. The green points correspond to the roots of the η function on the strip $\sigma = 1$, i.e., $0.9999948741 + i18.13024288$ (0.0010048257555), $0.9991999894 + i27.19393854$ (0.0011775300376), and $1.0007632157 + i36.25763092$ (0.0016708950835). The non-trivial zeroes of the ζ function are displayed as red points at the locations $0.4994029097 + i14.13722210$ (0.0001929922065), $0.5022082300 + i21.02339177$ (0.0013496548612), $0.4972257073 + i25.01157078$ (0.0016580104796), $0.4982199803 + i30.42602791$ (0.0010040109449), $0.4998933667 + i32.93208933$ (0.0043031376534), $0.4975621602 + i37.58347713$ (0.0046015734518), and $0.5006466505 + i40.91937548$ (0.0023928247564).

A major drawback we encountered with the η function is the computational time it requires to get a good approximation of the function values $\eta(s)$ for the given $s \in \mathbb{C}$. In particular, we used the partial sums from Equations (26) and (27), given by

$$\eta_{\text{Re}}^{(L)}(\sigma, t) = \sum_{n=1}^L \frac{(-1)^{n+1}}{n^\sigma} \cos(t \ln n), \quad (31)$$

and

$$\eta_{\text{Im}}^{(L)}(\sigma, t) = \sum_{n=1}^L \frac{(-1)^{n+1}}{n^\sigma} \sin(t \ln n). \quad (32)$$

with $L = 10000$, so that the approximation of η is given by

$$\hat{\eta}(s) = \eta_{\text{Re}}^{(L)}(\sigma, t) - i\eta_{\text{Im}}^{(L)}(\sigma, t), \quad (33)$$

which is not the most efficient way. More precisely, the results of Figure 4 (right) were produced using one iteration of the PPPZ for $N = 10000000$, $K = 15$, and required 30941.12s (8.59475hrs) to complete. Note here that the choice of L is directly affecting the accuracy of the results of the PPPZ, i.e., for this L we obtained the zeroes within tolerance $Tol = 10^{-2}$.

APPPZ zeroes, $p = 1$, 35.68s, $Tol = 1e - 10$, $x (f(x))$
0.09999993692 (3.979408372e-15)
APPPZ zeroes, $p = 2$, 12.83s, $Tol = 1e - 10$, $\mathbf{x} (f(\mathbf{x}))$
[0.1000009595, 0.1000012193] (2.407409327e-12)
APPPZ zeroes, $p = 3$, 21.23s, $Tol = 1e - 10$, $\mathbf{x} (f(\mathbf{x}))$
[0.1000069522, 0.1000008998, 0.09999654371] (6.108910006e-11)
APPPZ zeroes, $p = 4$, 2.00s, $Tol = 1e - 10$, $\mathbf{x} (f(\mathbf{x}))$
[0.1000019751, 0.1000017901, 0.1000052587, 0.09999698607] (4.384352667e-11)
APPPZ zeroes, $p = 5$, 433.31s, $Tol = 1e - 10$, $\mathbf{x} (f(\mathbf{x}))$
[0.09999492185, 0.09999744148, 0.09999579656, 0.09999903142, 0.1000030794] (6.042370764e-11)
APPPZ zeroes, $p = 10$, 2174.67s, $Tol = 1e - 4$, $\mathbf{x} (f(\mathbf{x}))$
[0.1042333147, 0.09891379454, 0.09843709304, 0.09784912086, 0.09974686875, 0.1048708919, 0.09828548259, 0.1037441446, 0.1016098485, 0.1043649247] (8.856178743e-05)

Table 3: The APPPZ algorithm for the function $f(\mathbf{x}) = \sum_{i=1}^p (x_i - 0.1)^2$, $\mathbf{x} = [x_1, \dots, x_p] \in \mathbb{R}^p$, which has a single zero at the point $\boldsymbol{\xi} = [0.1, \dots, 0.1]$. Results for $p = 1, 2, 3, 4$, and 5 , (10 iterations, $Q = 0.5$), and $p = 10$ (5 iterations, $Q = 1$). In all cases we used $K = 10$, and $N = 1000$.

3.4 Examples: multivariate real functions

Consider the multivariate function $f(\mathbf{x}) = \sum_{i=1}^p (x_i - 0.1)^2$, $\mathbf{x} = [x_1, \dots, x_p]^T \in \mathcal{W} = \{\mathbf{x} : -1 < x_i < 1, i = 1, 2, \dots, p\} \subset \mathbb{R}^p$, which has a single zero at the point $\boldsymbol{\xi} = [0.1, \dots, 0.1]^T$. We investigate the behavior of the PPPZ for this function as the dimension p increases. In Table 3 we present results of the APPPZ for $p = 1, 2, 3, 4$, and 5 , (10 iterations, $Q = 0.5$), and $p = 10$ (5 iterations, $Q = 1$). In all cases we used $K = 10$, and $N = 1000$. Note that all zeroes are recovered well, regardless of the specific dimension p .

As an example of optimization, we illustrate maximum likelihood estimation (MLE) of a multivariate normal model for different dimensions. More precisely, consider the unnormalized, p -variate standard normal $N_p(\mathbf{1}, \mathbf{I}_p)$, i.e., we will optimize the function

$$f(\mathbf{x}) = \exp \left\{ -\frac{1}{2} \|\mathbf{x} - \mathbf{1}\|^2 \right\},$$

for all $\mathbf{x} \in \mathcal{W} = \{\mathbf{x} : 0 < x_i < 2, i = 1, 2, \dots, p\} \subset \mathbb{R}^p$, where $\mathbf{1} \in \mathbb{R}^p$, denotes the unit vector $\mathbf{1} = [1, \dots, 1]^T$. As rudimentary as this example is, it provides additional insight on the performance of the APPPZ, and in particular, when the partial derivatives are "not known" in closed form for the multivariate, real-valued function under consideration. In Table 4 we present results of the APPPZ on the function $g(\mathbf{x}) = \sum_{i=1}^p \left| \widehat{\frac{\partial f(\mathbf{x})}{\partial x_i}} \right|$ (see Equation 20), for $p = 1, 2, 3, 4$ and 5 , with $K = 10$, $Q = 1$, and $N = 1000$. In all cases, the single point of maximum is attained at the unit vector $\boldsymbol{\xi} = \mathbf{1}$, with the maximum value given by $f(\boldsymbol{\xi}) = 1$, as anticipated.

Now consider the function $f(x, y) = (\sin(x/20) + \cos^2(x))(\sin(y/20) + \cos^2(y))$, $(x, y) \in \mathcal{W} = [-10, 10]^2 \subset \mathbb{R}^2$. The surface is displayed in Figure 5 (left), where we can see that

APPPZ zeroes, $p = 1$, 20.61s, $Tol = 1e - 5$, $x (f(x))$
0.9999999193 (2.997602166e-08)
APPPZ zeroes, $p = 2$, 55.93s, $Tol = 1e - 5$, $\mathbf{x} (f(\mathbf{x}))$
[1.000000055, 1.000000257] (4.130029652e-07)
APPPZ zeroes, $p = 3$, 946.64s, $Tol = 1e - 5$, $\mathbf{x} (f(\mathbf{x}))$
[1.000000484, 0.9999971188, 1.000002157] (5.573319584e-06)
APPPZ zeroes, $p = 4$, 10546.01s, $Tol = 1e - 04$, $\mathbf{x} (f(\mathbf{x}))$
[0.9996077, 1.000057, 0.9995982, 0.9998747] (0.0009759304476)
APPPZ zeroes, $p = 5$, 7262.19s, $Tol = 0.001$, $\mathbf{x} (f(\mathbf{x}))$
[0.9981542, 0.9949539, 1.000481, 1.000696, 0.9982167] (0.00985266202)

Table 4: The APPPZ algorithm for the function $f(\mathbf{x}) = \exp\{-\frac{1}{2}\|\mathbf{x} - \mathbf{1}\|^2\}$, $\mathbf{x} = [x_1, \dots, x_p] \in \mathbb{R}^p$, which has a single maximum at the unit vector $\boldsymbol{\xi} = \mathbf{1} = [1, \dots, 1]^T$, with maximum value $f(\boldsymbol{\xi}) = 1$. Results for $p = 1, 2, 3, 4$, and 5 . In all cases we used $K = 10$, $Q = 1$, and $N = 1000$.

the function attains its maximum at the boundary point $\boldsymbol{\xi} = [10, 10]^T$, but more importantly, there are many local minima and maxima that present significant challenges to existing methods, such as simulated annealing. We run the APPPZ for 5 iterations ($K = 10$, $Q = 0.5$, $N = 1000$, 31.32483hrs) and all the points of extrema are displayed in Figure 5 (right). Note that even in this nightmare scenario, the APPPZ is able to recover almost all the points of extrema simultaneously, with proposed global maximum at $[9.447049, 9.447047]$ ($4.511946372e - 06$) with $f(x, y) = 2.115531$, and proposed global minimum at $[9.447045, -7.877075]$ ($3.871347687e - 06$) with $f(x, y) = -0.5573836$.

4 Concluding Remarks

We presented a novel method for finding function zeroes utilizing point process theory. The APPPZ is able to obtain all zeroes of a real or complex function, and in many cases in a single iteration. Understanding the zeros of a function helps analyze its behavior, since the number and location of zeroes can indicate how the function grows or changes. Zeroes of a function are vital for solving equations, graphing, and analyzing real-world problems across various disciplines.

The choice of K greatly influences the effectiveness of the APPPZ algorithm. One approach that is currently explored in order to refine the proposed algorithm, involves treating K as a random variable, e.g., take $K \sim \text{Gamma}(a, \beta)$, $a, \beta > 0$. In this case, the intensity of the IPPP of Equation (10) becomes a random intensity (a random field), and the resulting random measure is known as a Cox point process (see [34], and the references therein). A Cox random measure essentially replaces the independence assumption of the Poisson point process with conditional independence, i.e., the numbers of points over disjoint regions are not necessarily independent. In Figure 6 we consider the zeroes of $f(x) = \cos(x)$, over the window $\mathcal{W} = [-10, 10]$, and present 1000 realizations (left plot) of the random intensity function $\lambda_K(\mathbf{x})$ ($Q = 0.5$), with source of randomness the parameter $K \sim \text{Gamma}(5, 2)$. The plot on the right presents 95% envelopes of the random intensity, as well as its mean.

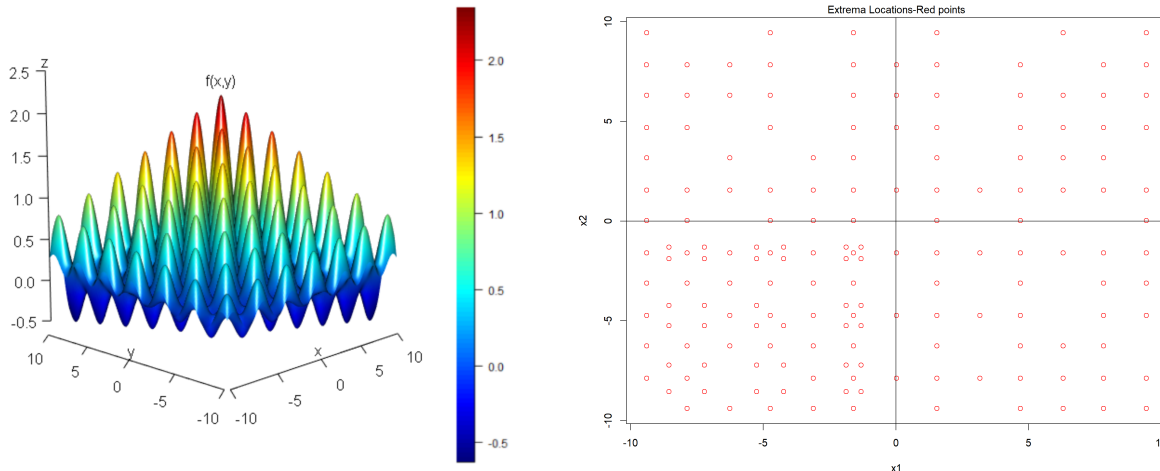


Figure 5: (left) The function $f(x, y) = (\sin(x/20) + \cos^2(x))(\sin(y/20) + \cos^2(y))$, $(x, y) \in \mathcal{W} = [-10, 10]^2 \subset \mathbb{R}^2$. (right) The APPPZ results from 5 iterations ($K = 10$, $Q = 0.5$, $N = 1000$, 31.32483hrs). All the points of extrema are displayed as red circles.

As expected, the intensity is exemplified about the zeroes of the function.

Several modifications and applications of the presented methods will be considered in the future, including a hierarchical Bayesian modeling approach to help the APPPZ select appropriate values of N , K and Q , automatically, in order to increase its performance in terms of accuracy and speed. These results are of great interest and will be presented elsewhere.

Acknowledgements

I am grateful to Professor Stamatis Dostoglou, Department of Mathematics, University of Missouri, for his constructive comments and suggestions on an earlier version of the manuscript.

References

- [1] I. Ba, J. F. Coeurjolly, and F. Cuevas-Pacheco. Pairwise interaction function estimation of stationary Gibbs point processes using basis expansion. *The Annals of Statistics*, 51(3):1134–1158, 2023.
- [2] A. Baddeley, E. Rubak, and R. Turner. *Spatial point patterns: methodology and applications with R*, volume 1. CRC press Boca Raton, 2016.
- [3] A. Baddeley, T. M. Davies, M. L. Hazelton, S. Rakshit, and R. Turner. Fundamental problems in fitting spatial cluster process models. *Spatial Statistics*, 52:100709, 2022.

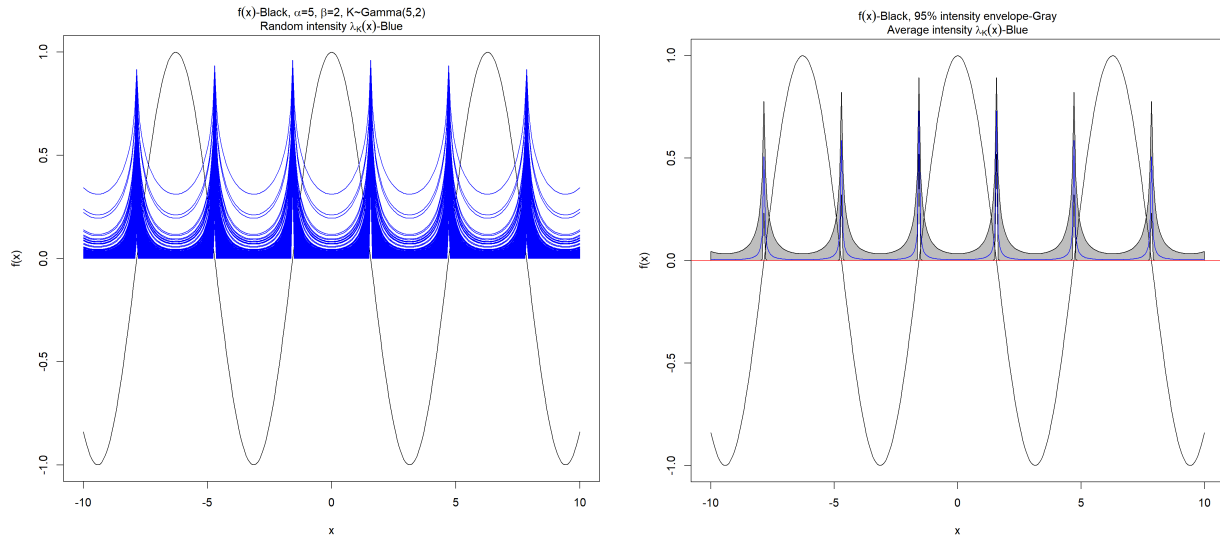


Figure 6: The function $f(x) = \cos(x)$, over the window $W = [-10, 10]$ (black color). We present 1000 realizations (left plot, blue color) of the random intensity function $\lambda_K(\mathbf{x})$ ($Q = 0.5$), with source of randomness the parameter $K \sim \text{Gamma}(5, 2)$. The plot on the right presents 95% envelopes of the random intensity (gray color), as well as its mean (blue color).

- [4] O. Barndorff-Nielsen. *Information and exponential families: in statistical theory*. John Wiley & Sons, 2014.
- [5] A. Benfenati, G. Borghi, and L. Pareschi. Binary interaction methods for high dimensional global optimization and machine learning. *Applied Mathematics & Optimization*, 86(1):9, 2022.
- [6] D. Bertsekas. *Convex optimization algorithms*. Athena Scientific, 2015.
- [7] P. Borwein. An efficient algorithm for the Riemann zeta function. In *Canadian Mathematical Society Conference Proceedings*, volume 27, pages 29–34, 2000.
- [8] A. Brochard, B. Błaszczyszyn, S. Zhang, and S. Mallat. Particle gradient descent model for point process generation. *Statistics and Computing*, 32(3):49, 2022.
- [9] A. Chakraborty and A.E. Gelfand. Measurement error in spatial point patterns. *Bayesian Analysis*, 5:97–122, 2010.
- [10] J. Chen, A. C. Micheas, and S. H. Holan. Bayesian modeling and decision theory for non-homogeneous poisson point processes. *Spatial Statistics*, 36:100412, 2020.
- [11] D. Chiu, S. N. and Stoyan, W. S. Kendall, and J. Mecke. *Stochastic geometry and its applications*. John Wiley & Sons, 2013.
- [12] N.A.C. Cressie. *Statistics for Spatial Data*. Wiley, New York, rev. ed. 1993 edition, 1991.

- [13] O. Cronie and M. N. M. Van Lieshout. A non-model-based approach to bandwidth selection for kernel estimators of spatial intensity functions. *Biometrika*, 105(2):455–462, 2018.
- [14] O. Cronie, M. Moradi, and C. AN Biscio. A cross-validation-based statistical theory for point processes. *Biometrika*, 111(2):625–641, 2024.
- [15] D. J. Daley and D. Vere-Jones. *An Introduction to the Theory of Point Processes, Volume I: Elementary Theory and Methods*. 2nd Edition, Springer, New York, 2005.
- [16] D. J. Daley and D. Vere-Jones. *An introduction to the theory of point processes: volume II: general theory and structure*. Springer Science & Business Media, 2007.
- [17] P. J. Diggle. *Statistical analysis of spatial and spatio-temporal point patterns*. CRC press, 2013.
- [18] U. M. Diwekar. *Introduction to applied optimization*, volume 22. Springer Nature, 2020.
- [19] A. E. Gelfand, P. J. Diggle, M. Fuentes, and P. Guttorp, editors. *Handbook of Spatial Statistics*. CRC, Boca Raton, 2010.
- [20] J. A. González, J. Dvořák, T. Mrkvička, and J. Mateu. A nonparametric test of independence between the second-order structure of point patterns and covariates. *Statistics and Computing*, 35(5):133, 2025.
- [21] Y. Guan and H. Wang. Sufficient dimension reduction for spatial point processes directed by gaussian random fields. *Journal of the Royal Statistical Society Series B: Statistical Methodology*, 72(3):367–387, 2010.
- [22] J. Guillera and J. Sondow. Double integrals and infinite products for some classical constants via analytic continuations of Lerch’s transcendent. *The Ramanujan Journal*, 16(3):247–270, 2008.
- [23] J. Illian, H. Penttinen, A. and Stoyan, and D. Stoyan. *Statistical analysis and modelling of spatial point patterns*. John Wiley & Sons, 2008.
- [24] A. Karr. *Point processes and their statistical inference*. Routledge, 2017.
- [25] Y. Kindap and S. Godsill. Point process simulation of generalised hyperbolic lévy processes. *Statistics and Computing*, 34(1):33, 2024.
- [26] M. J. Kochenderfer and T. A. Wheeler. *Algorithms for optimization*. Mit Press, 2019.
- [27] C. Kresin and F. Schoenberg. Parametric estimation of spatial-temporal point processes using the stoyan-grabarnik statistic. *Annals of the Institute of Statistical Mathematics*, 75(6):887–909, 2023.
- [28] C. Lantuéjoul. *Geostatistical simulation: models and algorithms*. Number 1139. Springer Science & Business Media, 2001.

- [29] F. Lavancier, J. Møller, and E. Rubak. Determinantal point process models and statistical inference. *Journal of the Royal Statistical Society Series B: Statistical Methodology*, 77(4):853–877, 2015.
- [30] A. B. Lawson and D. G. Denison. *Spatial cluster modelling*. Chapman and Hall/CRC, 2002.
- [31] P.A. W. Lewis and G. S. Shedler. Simulation of nonhomogeneous poisson processes by thinning. *Naval research logistics quarterly*, 26(3):403–413, 1979.
- [32] A. C. Micheas. Hierarchical Bayesian modeling of marked non-homogeneous Poisson processes with finite mixtures and inclusion of covariate information. *Journal of Applied Statistics*, 41(12):2596–2615, 2014.
- [33] A. C. Micheas. Cox point processes: why one realisation is not enough. *International Statistical Review*, 87(2):306–325, 2019.
- [34] A C. Micheas. Random mixture Cox point processes. *Annals of the Institute of Statistical Mathematics*, 77:289–330, 2025.
- [35] J. Møller. *Spatial Statistics and Computational Methods. Lecture Notes in Statistics*. Springer-Verlag, New York, Inc., 2003.
- [36] J. Møller and R. P. Waagepetersen. *Statistical inference and simulation for spatial point processes*. CRC press, 2003.
- [37] P. Pedregal. *Introduction to optimization*, volume 46. Springer, 2004.
- [38] P. O. Perry and P. J. Wolfe. Point process modelling for directed interaction networks. *Journal of the Royal Statistical Society Series B: Statistical Methodology*, 75(5):821–849, 2013.
- [39] D. A. Pierre. *Optimization theory with applications*. Courier Corporation, 2012.
- [40] U. Sadana, A. Chenreddy, E. Delage, A. Forel, E. Frejinger, and T. Vidal. A survey of contextual optimization methods for decision-making under uncertainty. *European Journal of Operational Research*, 320(2):271–289, 2025.
- [41] J. Sondow. Zeros of the alternating zeta function on the line $\Re(s) = 1$. *The American mathematical monthly*, 110(5):435–437, 2003.
- [42] E. Spodarev. *Stochastic geometry, spatial statistics and random fields: asymptotic methods*, volume 2068. Springer, 2013.
- [43] X. Tang and L. Li. Multivariate temporal point process regression. *Journal of the American Statistical Association*, 118(542):830–845, 2021.
- [44] M. N. M. Van Lieshout. *Markov point processes and their applications*. World Scientific, 2000.

- [45] M. N. M. Van Lieshout. Non-parametric adaptive bandwidth selection for kernel estimators of spatial intensity functions. *Annals of the Institute of Statistical Mathematics*, 76(2):313–331, 2024.
- [46] W. Wu and A C. Micheas. Modeling Fourier expansions using point processes on the complex plane with applications. *Communications in Statistics-Simulation and Computation*, 53(5):2207–2224, 2022.
- [47] W. Wu and A C. Micheas. A new construction of covariance functions for Gaussian random fields. *Sankhya A*, 86(1):530–574, 2024.
- [48] C. Y. Yau and J. M. Loh. A generalization of the Neyman–Scott process. *Statistica Sinica*, pages 1717–1736, 2012.
- [49] J. Zhuang, T. Wang, and K. Kiyosugi. Detection and replenishment of missing data in marked point processes. *Statistica Sinica*, 30(4):2105–2130, 2020.